



# Combined Effects of $f(R)$ Gravity and Massive Neutrinos on the Turnaround Radii of Dark Matter Halos

Jounghun Lee<sup>1</sup> and Marco Baldi<sup>2,3,4</sup> <sup>1</sup> Astronomy Program, Department of Physics and Astronomy, Seoul National University, Seoul 08826, Republic of Korea; [jounghun@astro.snu.ac.kr](mailto:jounghun@astro.snu.ac.kr)<sup>2</sup> Dipartimento di Fisica e Astronomia, Alma Mater Studiorum Università di Bologna, viale Bertini Pichat, 6/2, I-40127 Bologna, Italy<sup>3</sup> INAF-Osservatorio Astronomico di Bologna, via Ranzani 1, I-40127 Bologna, Italy<sup>4</sup> INFN-Sezione di Bologna, viale Bertini Pichat 6/2, I-40127 Bologna, Italy

Received 2022 July 18; revised 2022 September 10; accepted 2022 September 23; published 2022 October 21

## Abstract

We present a new statistics based on the turnaround radii of cluster halos to break the dark sector degeneracy between the  $\Lambda$ CDM model and the alternative ones with  $f(R)$  gravity and massive neutrinos ( $\nu$ ) characterized by the strength of the fifth force,  $|f_{R0}|$ , and the total neutrino mass,  $M_\nu$ . Analyzing the Rockstar halo catalogs at the present epoch from the DUSTGRAIN-*pathfinder*  $N$ -body simulations performed for four different cosmologies, namely,  $\Lambda$ CDM ( $|f_{R0}| = 0$ ,  $\sum m_\nu = 0.0$  eV), fR6 ( $|f_{R0}| = 10^{-6}$ ,  $\sum m_\nu = 0.0$  eV), fR6+0.06 eV ( $|f_{R0}| = 10^{-6}$ ,  $\sum m_\nu = 0.06$  eV), and fR5+0.15 eV ( $|f_{R0}| = 10^{-5}$ ,  $\sum m_\nu = 0.15$  eV), which are known to yield very similar conventional statistics to one another. For each model, we select those cluster halos that do not neighbor any other larger halos in their bound zones and construct their bound-zone peculiar velocity profiles at  $z = 0$ . Then, we determine the radial distance of each selected halo at which the bound-zone velocity becomes equal to the recession speed of the Hubble flow as its turnaround radius, and evaluate the cumulative probability distribution of the ratios of the turnaround radii to the virial counterparts,  $P(r_t/r_v \geq \alpha)$ . The degeneracy between the fR6 and fR5+0.15 eV models is found to be readily broken by the  $10\sigma_{\Delta P}$  difference in the value of  $P(\alpha = 4)$ , while the  $3.2\sigma_{\Delta P}$  difference between the  $\Lambda$ CDM and fR6+0.06 eV models is detected in the value of  $P(\alpha = 8.5)$ . It is also found that the four models yield smaller differences in  $P(\alpha)$  at higher redshifts.

*Unified Astronomy Thesaurus concepts:* [Cosmological models \(337\)](#); [Large-scale structure of the universe \(902\)](#)

## 1. Introduction

The turnaround radius of a dark matter (DM) halo is a characteristic distance scale at which the velocity field around the halo has a vanishingly small value in the radial direction due to the complete counterbalance between its inward gravity and the outward repulsion of the Hubble flow. Even though the turnaround radius is a property of a highly nonlinear structure, its value can in principle be theoretically predictable from the first principles as far as the halo forms through the spherically symmetric gravitational collapse process (Pavlidou et al. 2014; Pavlidou & Tomaras 2014). This advantageous aspect of the turnaround radius has motivated many authors to examine its potential as a probe of cosmology. For example, Pavlidou & Tomaras (2014) analytically evaluated the upper limit on the turnaround radii for the standard  $\Lambda$ CDM cosmology, where the gravitational law is described by Einstein's general relativity (GR), the present acceleration of the universe is driven by the cosmological constant ( $\Lambda$ ) with equation of state  $w = -1$ , and the most dominant matter content is the collisionless cold DM (CDM) particles having negligibly low speed at the moment of their decoupling.

What Pavlidou & Tomaras (2014) proved was that the spherical upper limit on the turnaround radii sensitively depends on the amount of  $\Lambda$  (see also Pavlidou et al. 2014; Bhattacharya & Tomaras 2017) and thus that a bound violation, if observed to occur, could in principle challenge the  $\Lambda$ CDM cosmology. Here, a bound violation is a term coined by Pavlidou & Tomaras (2014) to

describe an event of observing a cosmic structure whose turnaround radius is exceeding the analytically found *spherical* upper limit of the  $\Lambda$ CDM cosmology. Later, Lopes et al. (2018) theoretically proved that the upper limit of the turnaround radii can be used to detect the presence of modified gravity (MG; Clifton et al. 2012, for a review), which has an effect of significantly increasing the turnaround radii (see also Lopes et al. 2019).

The aforementioned theoretical works were based on the simple top-hat spherical dynamics (Gunn & Gott 1972), from which the real gravitational dynamics were in fact well known to depart (e.g., Bond & Myers 1996). To take into account the nonspherical nature of gravitational collapse for the determination of the turnaround radii and their upper limit, the numerical experiments had to be employed (Pavlidou & Tomaras 2014). For instance, Lee & Yepes (2016) used a high-resolution  $N$ -body simulation to measure the turnaround radii of DM halos located in the cosmic web (Bond et al. 1996) and demonstrated that the anisotropic merging along the filamentary structures has an effect of enlarging the turnaround radii. Their result implied that the occurrence of a bound violation is not unconditionally prohibited but occasionally possible even in the  $\Lambda$ CDM cosmology since the numerically determined nonspherical upper limit on the turnaround radii turned out to be higher than the analytically predicted spherical limit (see also Bhattacharya & Tomaras 2021; Faraoni 2021; Giusti & Faraoni 2021).

Nevertheless, the usefulness of the turnaround radii as a cosmological probe is not necessarily undermined by the fact that their upper limit cannot be treated in a purely analytical way. Lee & Li (2017) numerically found that it becomes significantly more probable for a bound violation to occur in the presence of MG and thus that the frequency of the

occurrence of the bound violations should be a powerful test of GR. Their claim was supported by several follow-up works that theoretically proved that the alternative cosmologies including quintessence dark energy, scalar-tensor theory, and phantom brane world induce more frequent occurrences of the bound violations (Bhattacharya & Kousvos 2017; Bhattacharya & Tomaras 2017; Lopes et al. 2018; Nojiri et al. 2018; Lopes et al. 2019).

In light of the aforementioned works that disclosed the sensitivity of the turnaround radii especially to the nature of gravity, we attempt here to numerically explore if the turnaround radii are capable of discriminating the alternative MG models that have been known to be degenerate with the  $\Lambda$ CDM cosmology by the conventional statistics such as the linear and nonlinear density power spectra, cluster mass function, halo bias factor, and redshift distortion effect (Baldi et al. 2014; Hagstotz et al. 2019). For this exploration, our analysis will focus on a particular class of MG models, namely, the  $\nu$ CDM+ $f(R)$  gravity model, where the massive neutrinos ( $\nu$ ) with nonzero total mass  $\sum m_\nu$  are present along with CDM and the apparent acceleration of spacetime at the present epoch is caused by the failure of GR on the cosmological scales (see De Felice & Tsujikawa 2010, for a review).

The gravitational dynamics of this alternative model is dictated by the modified Einstein–Hilbert action in which some specified function,  $f(R)$ , substitutes for the Ricci scalar  $R$ . An additional fifth force is generated by its extra degree of freedom,  $f_R \equiv df/dR$ , dubbed the scalaron, whose absolute value at the present epoch,  $|f_{R0}|$ , quantifies how strong fifth force the  $f(R)$  gravity can exert (see Hu & Sawicki 2007, and references therein). Although the Chameleon shielding mechanism turns off the fifth force in the high-density regions, the overall effect of  $f(R)$  gravity alone is to enhance the density growth via its fifth force compared with the  $\Lambda$ CDM case (see Khoury & Weltman 2004, and references therein). However, in the presence of massive neutrinos that have an effect of suppressing the density growth (e.g., see Lesgourgues & Pastor 2014), this effect of  $f(R)$  gravity can be severely attenuated. It was indeed numerically shown that a proper combination of  $\sum m_\nu$  with  $|f_{R0}|$  can make a  $\nu$ CDM+ $f(R)$  gravity model yield very similar conventional statistics to the  $\Lambda$ CDM case (Baldi et al. 2014; Hagstotz et al. 2019).

In this Paper, we will provide numerical evidence supporting that the turnaround radii may break this degeneracy between the  $\Lambda$ CDM and  $\nu$ CDM+ $f(R)$  gravity models. The organization of this paper is as follows. In Section 2, we briefly review the previously developed algorithm for the estimation of the turnaround radii of DM halos. In Section 3, we describe the numerical data used for our analysis and explain how well the cumulative probability of the turnaround radii of DM halos differentiates between the  $\Lambda$ CDM and  $\nu$ CDM+ $f(R)$  gravity models. In Section 4, we summarize the results and discuss the caveats and limitations of our statistics as a cosmological discriminator.

## 2. A Review of the Turnaround Radius Estimator Algorithm

The neighborhood around a DM halo is often divided into three distinct sectors called the infall, bound, and Hubble zones, depending on which effect is more dominant between the gravity and the cosmic expansion. The infall (Hubble) zone corresponds to the radial distance range,  $r \leq 2r_v$  ( $r \geq 10r_v$ ), in

which the effect of the gravitational attraction of the halo on the radial components of the peculiar velocities,  $v_r$ , completely surpasses (surrenders) that of the receding Hubble flow, where  $r_v$  is the halo virial radius. Meanwhile, the in-between bound zone corresponds to the region where the two competing forces are so well balanced that  $v_r$  can be tractable in the linear perturbation theory.

Falco et al. (2014) showed that the profile of the radial components of the peculiar velocity field in the bound zone,  $v_r(r)$ , around the cluster halos with virial mass  $M_v \gtrsim 0.5 \times 10^{14} h^{-1} M_\odot$  has a universal shape, well approximated by the following formula

$$\frac{v_r(r)}{V_c} = -A \left( \frac{r_v}{r} \right)^n, \quad (1)$$

where two adjustable parameters,  $A$  and  $n$ , quantify the amplitude and slope of the profile, respectively, and  $V_c$  is the circular velocity equivalent to  $(GM_v/r_v)^{1/2}$ . The negative sign in the right-hand side of Equation (1) indicates that the bound-zone neighbors still feel the net gravitational force of the halo. From here on, we let  $v_r(r)$  exclusively denote the profile of the radial components of the peculiar velocity field in the bound zone around the cluster halos and call it the *bound-zone velocity profile*.

Falco et al. (2014) claimed the *universality* of Equation (1) based on their numerical finding that the stacked bound-zone velocity profiles over the cluster halos have a constant slope and amplitude, being almost independent of the cluster masses and redshifts. It was also found by Falco et al. (2014) that not only the stacked ones but also the bound-zone velocity profiles,  $v_r(r)$ , around individual cluster halos follow the above formula well, although the best-fit values of  $A$  and  $n$  exhibited substantial scatters around the mean values. The pioneering work of Falco et al. (2014) motivated further numerical investigations of the bound-zone velocity profiles around the cluster halos, which all confirmed the validity of Equation (1) for the description of  $v_r(r)$  (Lee et al. 2015; Lee 2016; Lee & Yepes 2016; Lee 2018; Hansen et al. 2020).

Lee & Yepes (2016) demonstrated with the help of  $N$ -body simulations that the best-fit values of  $A$  and  $n$  in Equation (1) depend on the halo environments and that the best agreements between the numerically obtained  $v_r(r)$  and Equation (1) can be achieved for the case that the cluster halos are located in the relatively low-density environments, having no larger neighbor halos in their bound zones. They also showed that even when  $v_r(r)$  is constructed not directly from the DM particles but only from the distinct neighbor halos in the bound zones, it is well described by Equation (1), proving the feasibility of the observational application of Equation (1) to real data. Lee (2016) confirmed the universality of Equation (1), showing that the best-fit values of  $A$  and  $n$  in Equation (1) are quite insensitive to the variation of the key cosmological parameters,  $\sigma_8$  and  $\Omega_m$ . It was also found by Lee (2016) that Equation (1) is valid even on the lower mass scales corresponding to the group-size halos,  $5 \times 10^{12} \leq M_v/(h^{-1} M_\odot) \leq 10^{13}$ , as far as the halos are located in the isolated regions.

Lee et al. (2015) proposed an algorithm based on Equation (1) to estimate the turnaround radii,  $r_t$ , of the cluster halos, calling it the turnaround radius estimator (TRE). By definition, the magnitude of the bound-zone velocity,  $v_r$ , at  $r_t$  becomes equal to the speed of the Hubble flow,  $H_0 r_t$ . By Equation (1), however,  $|v_r(r_t)|$  is nothing but  $A[r_v/r_t]^n$ . Given

that  $A$  and  $n$  have constant values, the turnaround radius of a cluster halo can be estimated simply by solving the following equation:

$$A \left[ \frac{r_v}{r_t} \right]^n = \frac{H_0 r_t}{V_c}. \quad (2)$$

Lee & Li (2017) applied the TRE to the numerical data from a high-resolution  $N$ -body simulation and found that the TRE worked better when they used the best-fit values of  $A$  and  $n$  obtained separately for each cluster halo rather than using their constant mean values.

For the application of the TRE to the real clusters from observations, the critical issue to address was whether or not the values of  $A$  and  $n$  for the individual clusters could be obtained without measuring the bound-zone peculiar velocities. According to Falco et al. (2014), for those cluster halos embedded in cosmic filaments, it is possible to construct  $v_r(r)$  from limited information only on the redshift space positions of the bound-zone galaxies. Once  $v_r(r)$  is constructed for the filament clusters whose virial mass and radius are known, then the values of  $A$  and  $n$  can be readily obtained through fitting of  $v_r(r)$  to Equation (1). Lee (2018) applied this TRE to the local galaxy clusters located in the straight filamentary structures and successfully estimated their turnaround radii, validating its practical usefulness. In Section 3, we will apply the TRE to the numerical data for the investigation of the combined effects of  $f(R)$  gravity and massive neutrinos on the turnaround radii of the cluster halos.

### 3. Physical Analysis

The DUSTGRAIN-*pathfinder* simulation project aimed at keeping track of  $768^3$  CDM particles of individual mass  $8.1 \times 10^{10} h^{-1} M_\odot$  under the influence of  $f(R)$  gravity in the presence of massive neutrinos (Giocoli et al. 2018) on the periodic box of volume  $750^3 h^{-3} \text{Mpc}^3$ . The MG-GADGET encoded by Puchwein et al. (2013) was implemented for the computation of the Hu–Sawicki  $f(R)$  gravity (Hu & Sawicki 2007), while the incorporation of massive neutrinos was achieved via the particle-based routine programmed by Viel et al. (2010). See Giocoli et al. (2018) and Puchwein et al. (2013) for detailed information on the DUSTGRAIN-*pathfinder* project and MG-GADGET code, respectively. Among many  $\nu\text{CDM}+f(R)$  gravity models simulated by the DUSTGRAIN-*pathfinder*, we consider the following three, fR6 ( $|f_{R0}| = 10^{-6}$ ,  $\sum m_\nu = 0.0 \text{ eV}$ ), fR6+0.06 eV ( $|f_{R0}| = 10^{-6}$ ,  $\sum m_\nu = 0.06 \text{ eV}$ ), and fR5+0.15 eV with  $|f_{R0}| = 10^{-5}$  and  $\sum m_\nu = 0.15 \text{ eV}$  models. As mentioned in Section 1, it was shown by the previous works of Baldi et al. (2014) and Hagstotz et al. (2019) that the conventional statistics can hardly discriminate these three models from the  $\Lambda\text{CDM}$  cosmology, which was also simulated by the DUSTGRAIN-*pathfinder* project, setting the initial conditions at the Planck values (Planck Collaboration et al. 2016).

For each of the four models, i.e., the  $\Lambda\text{CDM}$  and the three  $\nu\text{CDM}+f(R)$  gravity cosmologies, Lee et al. (2022) identified the DM halos by applying the Rockstar algorithm (Behroozi et al. 2013) to the snapshot data of the DUSTGRAIN-*pathfinder* simulations. From the Rockstar halo catalogs at  $z=0$ , we extract the cluster-size distinct halos with  $M_v \geq 4.05 \times 10^{13} h^{-1} M_\odot$  enclosing 500 or more DM particles within their virial radii  $r_v$ . Among them, we select only those cluster halos that do not neighbor any higher-mass halos in

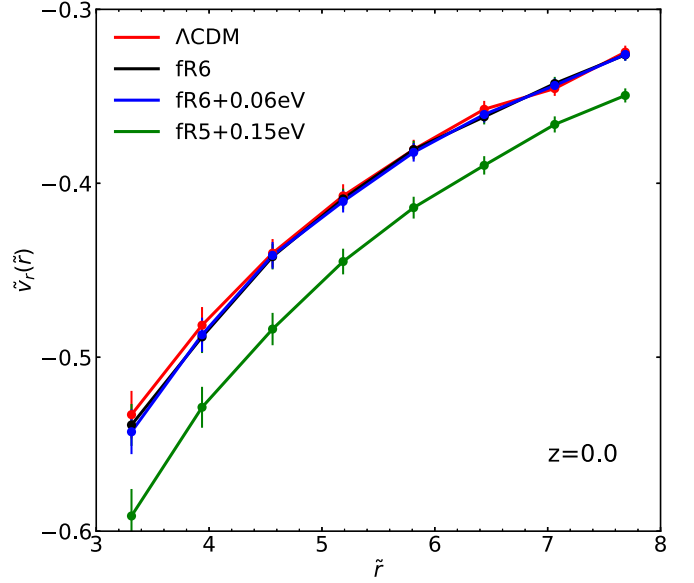


**Figure 1.** Bound-zone velocity profiles around the cluster halos with  $M_v \geq 4.05 \times 10^{13} h^{-1} M_\odot$  at  $z=0$  for four different cosmological models.

their bound zones. From here on, the selected cluster halos will be referred to as the host halos, for which we find the neighbor halos located in their bound zones and containing 20 or more DM particles. Then, we compute the radial components of the relative peculiar velocities of the bound-zone neighbors around each host as

$$v_r = \hat{r} \cdot (\mathbf{V}_h - \mathbf{V}_b), \quad (3)$$

where  $\mathbf{V}_h$  and  $\mathbf{V}_b$  denote the comoving peculiar velocities of a host halo and its bound-zone neighbor halo, respectively, and  $\hat{r}$  is the unit vector in the direction from the host halo center to the bound-zone neighbor separated by a distance  $r$ . The rescaled bound-zone velocities and separation distances,  $\tilde{v}_r$  and  $\tilde{r}$ , are defined as  $\tilde{v}_r \equiv v_r/V_c$  and  $\tilde{r} \equiv r/r_v$ , respectively. From here on, we will call  $\tilde{v}_r$  the bound-zone velocity profile, dropping the term, “rescaled,” unless otherwise stated.

Breaking up the bound-zone distance range of  $2 < \tilde{r} < 10$  into several intervals of equal length,  $\Delta\tilde{r} = 1$ , we take the average of  $\tilde{v}_r$  over those neighbors with  $\tilde{r}$  falling in each interval to determine the bound-zone velocity profile,  $\tilde{v}_r(r)$ , for each host. Then, we take its ensemble average over all of the hosts to determine the stacked bound-zone velocity profile,  $\langle \tilde{v}_r \rangle$ , the result of which is shown in Figure 1. As can be seen, the average bound-zone velocity profiles conspicuously differ between the fR5+0.15 eV and the other three models. The former case yields significantly higher values of  $|\langle \tilde{v}_r \rangle|$  in the whole range of  $\tilde{r}$  than the latter case, which must be caused by the difference in the strength of the fifth force between the two cases. This result implies that the free streaming of more massive neutrinos present in the fR5+0.15 eV model do not severely attenuate the effect of its stronger fifth force on the bound-zone velocity profiles.

We fit  $\langle \tilde{v}_r \rangle$  to Equation (1) by simultaneously adjusting  $A$  and  $n$  with the help of the  $\chi^2$  minimization method for each model. Table 1 lists their best-fit values in the third and fourth columns for the four cosmologies. Figure 2 compares the numerically obtained  $\langle \tilde{v}_r \rangle$  (black filled circles) to the analytic formula with the best-fit values of  $A$  and  $n$  (red solid lines), revealing the excellent agreements between the numerical and analytical

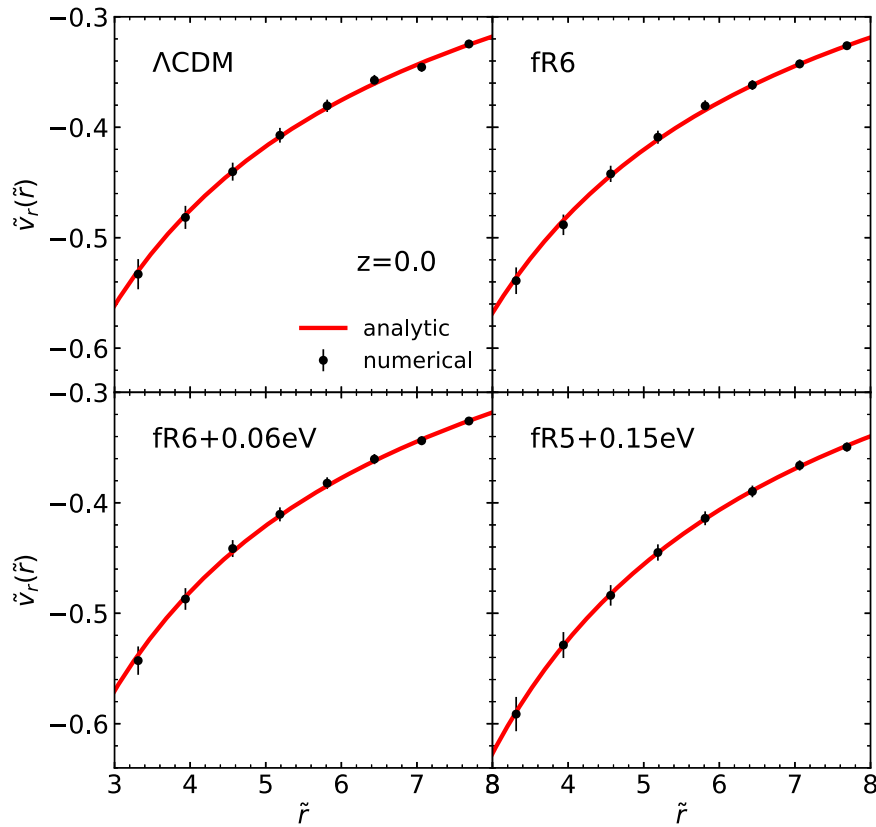


**Figure 2.** Comparison of the numerically obtained bound-zone velocity profiles (black filled circles) with the best-fit analytic formula (red solid lines) at  $z = 0$ .

**Table 1**  
Best Parameters and Probabilities of  $r_t \geq \alpha r_v$  at  $z = 0$

Cosmology	$N_h$	$A$	$n$	$P(\alpha = 4)$ ( $10^{-2}$ )	$P(\alpha = 8.5)$ ( $10^{-3}$ )
$\Lambda$ CDM	18188	$1.061 \pm 0.045$	$0.580 \pm 0.023$	$43.50 \pm 0.37$	$0.87 \pm 0.22$
fR6	19317	$1.086 \pm 0.041$	$0.590 \pm 0.021$	$43.69 \pm 0.36$	$0.50 \pm 0.16$
fR6+0.06 eV	18811	$1.096 \pm 0.043$	$0.595 \pm 0.021$	$43.61 \pm 0.37$	$0.11 \pm 0.08$
fR5+0.15 eV	19291	$1.245 \pm 0.053$	$0.625 \pm 0.035$	$53.74 \pm 0.36$	$1.37 \pm 0.28$

results. This result confirms the validity and usefulness of Equation (1) not only for the  $\Lambda$ CDM model but also for the  $\nu$ CDM+ $f(R)$  gravity models. Figure 3 plots the 68%, 95%, and 99% contours of  $\chi^2(A, n)$ , quantifying how significant the differences in the best values of  $A$  and  $n$  are between the fR5+0.15 eV and the other three models.

Recall that the fR5+0.15 eV model is very similar to the other three ones in the conventional statistics (Baldi et al. 2014). Especially the fR6 model has been shown to be almost indistinguishable from the fR5+0.15 eV, as the effect of the stronger fifth force,  $|f_{R0}| = 10^{-5}$  is so severely attenuated by the free streaming massive neutrinos with  $\sum m_\nu = 0.15$  eV that the palpable effect amounts only to that of  $|f_{R0}| = 10^{-6}$ . However, the average bound-zone velocity profile, unlike the aforementioned conventional statistics, is capable of disentangling the effect of the fifth force from that of the massive neutrinos, sensitively varying with the former, but not with the latter. Yet, given that the other three models still remain mutually indistinguishable even by  $\langle v_r(r) \rangle$ , we now investigate if any other statistics based on  $v_r(r)$  beyond its ensemble average can break the degeneracy among the other three models. Basically, we

consider the turnaround radii of the hosts as such statistics, and estimate them by applying the TRE reviewed in Section 2 to the individual bound-zone velocity profiles.

For each host, we fit the individual bound-zone velocity profile to Equation (1) and separately determine the best-fit values of  $A$  and  $n$ . While performing this fitting procedure, we exclude a small fraction of the hosts whose bound-zone velocity profiles fail to be fitted by Equation (1) due to the low number of their bound-zone neighbors. Table 1 lists the number of the hosts,  $N_h$ , whose  $v_r(r)$  matches Equation (1) for the four cosmologies in the second column. Plugging the best-fit values of  $A$  and  $n$  into Equation (2) and solving it, we estimate the turnaround radius,  $r_t$ , of each of the included hosts. Counting the host halos whose turnaround radii exceed  $\alpha r_v$  as a function of a dimensionless variable  $\alpha$ , we obtain the cumulative probability  $P(r_t \geq \alpha r_v)$ . To assess the errors,  $\sigma_P$ , in  $P(r_t \geq \alpha r_v)$ , we create 10,000 bootstrap resamples composed of equal numbers of the hosts and obtain the cumulative probabilities from each resample. The one standard scatter among the resamples from the average is taken as  $\sigma_P$ .

Figure 4 plots the cumulative probabilities,  $P(r_t \geq \alpha r_v)$ , with the bootstrap errors,  $\sigma_P$ , for the four models. As expected, the

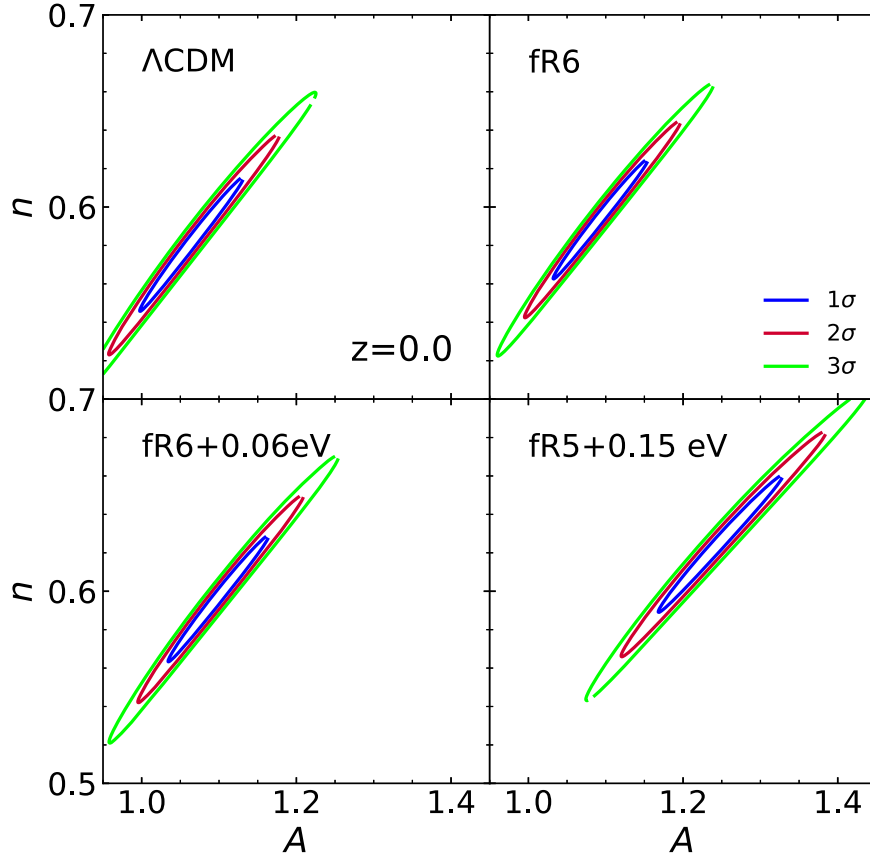


**Figure 3.** 68%, 95%, and 99% contours from the  $\chi^2$  statistics for two parameters,  $A$  and  $n$ , which characterize the analytic formula for the bound-zone velocity profiles, Equation (1), at  $z = 0$ .

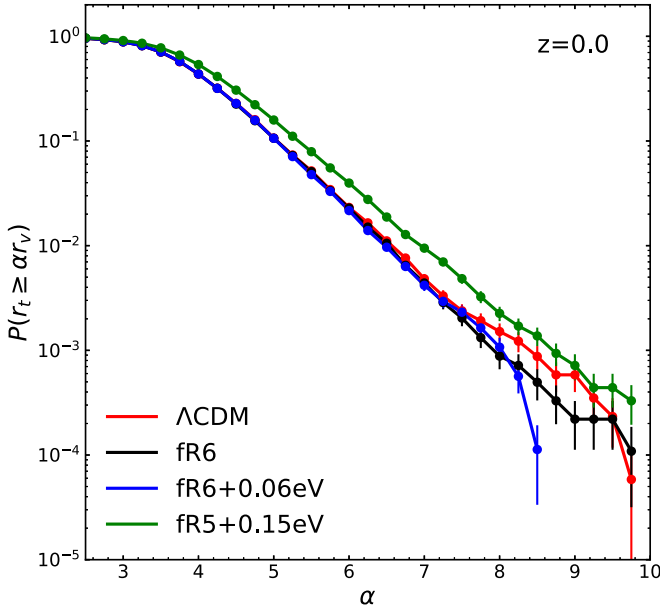


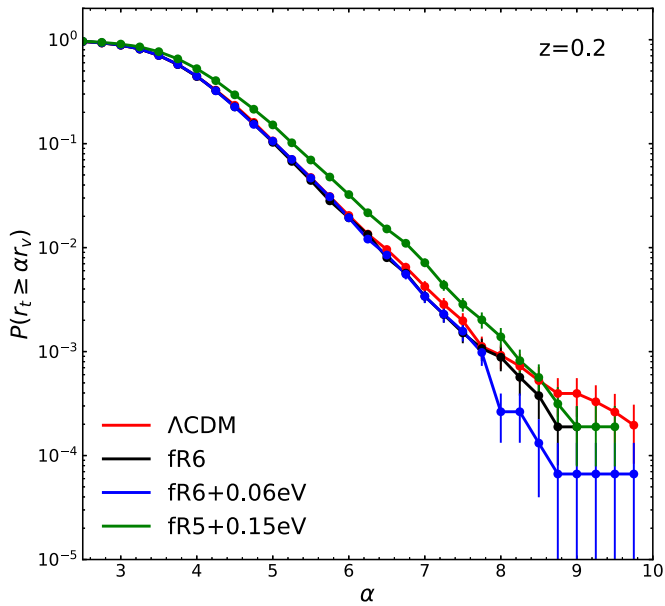
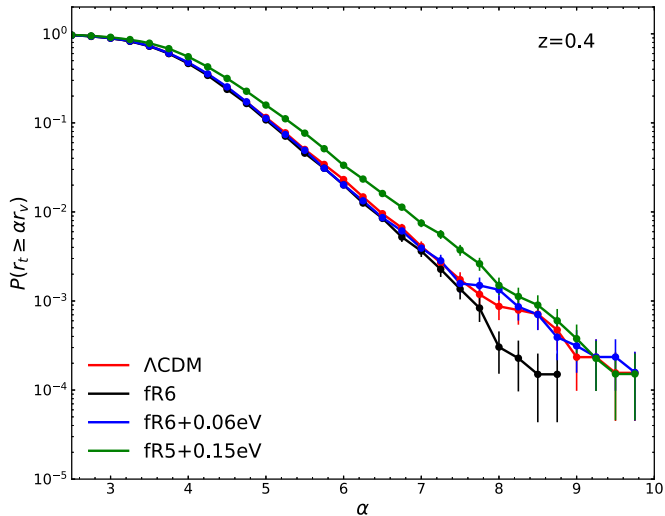
**Figure 4.** Cumulative probability function of the ratios of the turnaround radii to the virial counterparts at  $z = 0$ .

fR5+0.15 eV model yields the most conspicuously different  $P(r_t \geq \alpha r_v)$  from the other three models. The host halos in the fR5+0.15 eV model seem to have much larger turnaround radii than in the other three models, producing a 22% higher value of  $P(\alpha = 4)$ , corresponding to a  $10\sigma_{\Delta P}$  signal, where the

uncertainties,  $\sigma_{\Delta P}$ , associated with the measurement of the difference between the cumulative probabilities, are computed through the propagation of the bootstrap errors.

Regarding the other three models, they yield almost identical values of  $P(r_t \geq \alpha r_v)$  up to  $\alpha = 8$ . However, the two models,  $\Lambda$ CDM and fR6+0.06 eV, which are in fact indistinguishable by the conventional statistics (Baldi et al. 2014; Hagstotz et al. 2019), show different behaviors in the limit of  $\alpha > 8$ . The difference in the value of  $P(\alpha = 8.5)$  between the two models is found to be as high as  $3.2\sigma_{\Delta P}$  in spite of the strongest degeneracy between them, yielding the same value of  $\sigma_8$  (Baldi et al. 2014; Hagstotz et al. 2019). Table 1 lists  $P(\alpha = 4)$  and  $P(\alpha = 8.5)$  for the four cosmologies in the fifth and sixth columns. Noting that the fR6+0.06 eV model yields a smaller value of  $P(\alpha = 8.5)$  than the other models and that the fR6 model does not show any significant difference in the whole range of  $\alpha$  from the  $\Lambda$ CDM case; we suspect the following: even though the bound-zone velocity profiles are less sensitive to the presence of massive neutrinos, the effect of  $f(R)$  gravity combined with massive neutrinos on the turnaround radii is different from that of  $f(R)$  gravity alone especially for the case that the  $f(R)$  gravity is not strong enough to prostrate the effect of free streaming massive neutrinos.

We make the same analysis but of the cluster halos identified at two different redshifts,  $z = 0.2$  and  $0.4$  to see how  $P(\alpha)$  changes with redshifts, the results of which are shown in Figures 5 and 6, respectively. As can be seen,  $P(\alpha)$ , diminishes more rapidly with  $\alpha$  at higher redshifts. While the statistical significance of the difference in  $P(\alpha = 4)$  between the fR5 +0.15 eV and other three models is quite robust against the

Figure 5. Same as Figure 4 but at  $z = 0.2$ .Figure 6. Same as Figure 4 but at  $z = 0.4$ .

redshift variation, which in  $P(\alpha \geq 8)$  between the  $\Lambda$ CDM and fR6+0.06 eV models drops to  $2.3\sigma_{\Delta P}$  at  $z = 0.2$  and to a negligible level at  $z = 0.4$ . The low abundance of the cluster halos at higher redshifts contributes to the large uncertainties in  $P(\alpha)$ , rendering it inconclusive whether or not the strongest degeneracy between  $\Lambda$ CDM and fR6+0.06 eV can be broken by the turnaround radii of the cluster halos at  $z \geq 0.2$ .

#### 4. Summary and Conclusion

We have numerically demonstrated that the turnaround radii of cluster halos can in principle be useful to detect the effect of  $f(R)$  gravity attenuated by the presence of massive neutrinos. The samples of the cluster halos with  $M_v \geq 4.0 \times 10^{14} h^{-1} M_\odot$  at  $z=0$  were obtained from the DUSTGRAIN-*pathfinder* simulations (Giocoli et al. 2018) performed for four different cosmologies: the Planck  $\Lambda$ CDM and three  $\nu$ CDM+ $f(R)$  gravity models having different strengths of fifth force and total neutrino mass: fR6, fR6+0.06 eV, fR5+0.15 eV, which were known to be degenerate with the  $\Lambda$ CDM model and with one

another, yielding very similar conventional statistics (Baldi et al. 2014; Hagstotz et al. 2019).

For the determination of the turnaround radii,  $r_t$ , of the cluster halos at which the value of the peculiar velocity field becomes equal to the recession speed of the Hubble flow, we have employed the TRE developed by Lee et al. (2015), which in turn utilizes the universal analytic formula for the peculiar velocity profile in the bound zone around the cluster halos, put forth by Falco et al. (2014) for the  $\Lambda$ CDM case. Our comparison of the analytic formula with the average bound-zone velocity profile through the  $\chi^2$  statistics has confirmed its validity not only for the Planck  $\Lambda$ CDM but also for the three  $\nu$ CDM+ $f(R)$  gravity models. It has also revealed that the amplitudes and slopes of the bound-zone velocity profiles, quantified by their two adjustable parameters, significantly differ between the fR5+0.15 eV and other three models (Figures 1–3). This result implies that the bound-zone velocities of the cluster halos must be much more susceptible to the presence of the strong fifth force than to that of massive neutrinos and thus some statistics based on them may be useful to disentangle the former from the latter.

With the turnaround radii of the cluster halos estimated by the application of the TRE to the bound-zone velocity profiles of individual cluster halos, we have determined the cumulative probability distributions of the turnaround to virial radius ratios,  $P(r_t \geq \alpha r_v)$ . With the help of the bootstrap statistics, we have shown that the fR5+0.15 eV model can be plainly differentiated by  $P(r_t/r_v \geq 4)$  from the other three cases, with statistical significance as high as  $10\sigma_{\Delta P}$  (Figure 4). We have also detected a  $3.2\sigma_{\Delta P}$  difference in  $P(r_t/r_v \geq 8.5)$  between the  $\Lambda$ CDM and fR6+0.06 eV models, in spite of the strongest degeneracy between the two cases. Yet, given the low value of  $P(r_t/r_v \geq 8.5) \sim \mathcal{O}(10^{-4})$ , it is not conclusive whether the  $3.2\sigma_{\Delta P}$  difference in  $P(r_t/r_v \geq 8.5)$  between the  $\Lambda$ CDM and fR6+0.06 eV models is a real signal or just a spurious one produced by the shot noise. A larger sample of the massive cluster halos with  $r_t \geq 8r_v$  will be required to confirm the statistical significance of the difference in  $P(\alpha > 8)$  between the two models. It has been also shown that the significance of the difference between the fR5+0.15 eV and the other three models is robust against the variation of the redshifts from  $z = 0.0$  to 0.4 (Figures 5–6).

The advantage of using the turnaround radii estimated by the TRE to distinguish among the  $\Lambda$ CDM and  $\nu$ CDM+ $f(R)$  gravity models comes from the universality of the bound-zone velocity profile on which the TRE is based. As revealed by the previous works (Falco et al. 2014; Lee 2016), the shape of the bound-zone velocity profile is insensitive to the key cosmological parameters of the  $\Lambda$ CDM model. Thus, the variation of  $\sigma_8$  and  $\Omega_m$  in the  $\Lambda$ CDM model cannot produce the same effect on the turnaround radii as the  $\nu$ CDM+ $f(R)$  gravity. Furthermore, it does not require tracking down the redshift evolution of  $r_t$ , unlike the previously suggested statistics as a possible discriminator of the  $\nu$ CDM+ $f(R)$  gravity model such as the size evolutions of galaxy voids, nonlinear growth rates, and redshift distortions, evolution of the drifting average coefficient of the field cluster mass function, and high-order weak lensing statistics (Giocoli et al. 2018; Peel et al. 2018; Hagstotz et al. 2019; Wright et al. 2019; Ryu et al. 2020; Contarini et al. 2021).

It is, however, worth discussing the practical difficulties of our statistics. To detect a signal of the difference in  $P(\alpha \geq 8)$  strong enough to distinguish among the degenerate models, what is required is to measure the turnaround radii of as many galaxy clusters as possible in the local universe. However, as

shown in Lee (2018) and Hansen et al. (2020), the TRE is applicable only to those isolated galaxy clusters whose bound-zone neighbor galaxies exhibit a very high degree of anisotropy in their spatial distributions. Due to this limitation of the TRE, it would be difficult to obtain a large sample of the galaxy clusters with their turnaround radii measurable without information on the peculiar velocity field. Notwithstanding, we expect that the large peculiar velocity data set available from future galaxy surveys like The Large Synoptic Survey Telescope survey (Tyson 2002) should allow us to directly measure the turnaround radii of almost all of the galaxy clusters at low redshifts  $z \leq 0.2$ , making our statistics based on the turnaround radii to be practically useful as a powerful discriminator of the  $\nu$ CDM+ $f(R)$  gravity models.

J.L. acknowledges the support by Basic Science Research Program through the National Research Foundation (NRF) of Korea funded by the Ministry of Education (No. 2019R1A2C1083855). J.L. thanks S.Ryu for having been helpful in obtaining the Rockstar halo catalogs from the *Dustgrain-pathfinder* simulations. M.B. acknowledges support by the project “Combining Cosmic Microwave Background and Large Scale Structure data: an Integrated Approach for Addressing Fundamental Questions in Cosmology,” funded by the MIUR Progetti di Ricerca di Rilevante Interesse Nazionale (PRIN) Bando 2017—grant 2017YJYZAH. M.B. also acknowledges the use of computational resources from the parallel computing cluster of the Open Physics Hub at the Physics and Astronomy Department in Bologna (<https://site.unibo.it/openphysicshub/en>).

#### ORCID iDs

Jounghun Lee  <https://orcid.org/0000-0003-0522-4356>  
 Marco Baldi  <https://orcid.org/0000-0003-4145-1943>

#### References

- Baldi, M., Villaescusa-Navarro, F., Viel, M., et al. 2014, *MNRAS*, 440, 75  
 Behroozi, P. S., Wechsler, R. H., & Wu, H.-Y. 2013, *ApJ*, 762, 109  
 Bhattacharya, S., & Kousvos, S. R. 2017, *PhRvD*, 96, 104006  
 Bhattacharya, S., & Tomaras, T. N. 2017, *EPJC*, 77, 526  
 Bhattacharya, S., & Tomaras, T. N. 2021, *AnPhy*, 427, 168427  
 Bond, J. R., Kofman, L., & Pogosyan, D. 1996, *Natur*, 380, 603  
 Bond, J. R., & Myers, S. T. 1996, *ApJS*, 103, 1  
 Clifton, T., Ferreira, P. G., Padilla, A., et al. 2012, *PhR*, 513, 1  
 Contarini, S., Marulli, F., Moscardini, L., et al. 2021, *MNRAS*, 504, 5021  
 De Felice, A., & Tsujikawa, S. 2010, *LRR*, 13, 3  
 Falco, M., Hansen, S. H., Wojtak, R., et al. 2014, *MNRAS*, 442, 1887  
 Faraoni, V. 2021, *JPhCS*, 2156, 012017  
 Giocoli, C. M., Baldi, M., & Moscardini, L. 2018, *MNRAS*, 481, 2813  
 Giusti, A., & Faraoni, V. 2021, *PhRvD*, 103, 044049  
 Gunn, J. E., & Gott, J. R. 1972, *ApJ*, 176, 1  
 Hagstotz, S., Costanzi, M., Baldi, M., et al. 2019, *MNRAS*, 486, 3927  
 Hagstotz, S., Gronke, M., Mota, D. F., et al. 2019, *A&A*, 629, A46  
 Hansen, S. H., Hassani, F., Lombriser, L., et al. 2020, *JCAP*, 2020, 048  
 Hu, W., & Sawicki, I. 2007, *PhRvD*, 76, 064004  
 Khoury, J., & Weltman, A. 2004, *PhRvD*, 69, 044026  
 Lee, J. 2016, *ApJ*, 832, 123  
 Lee, J. 2018, *ApJ*, 856, 5  
 Lee, J., Kim, S., & Rey, S.-C. 2015, *ApJ*, 815, 43  
 Lee, J., & Li, B. 2017, *ApJ*, 842, 2  
 Lee, J., Ryu, S., & Baldi, M. 2022, arXiv:2206.03406  
 Lee, J., & Yepes, G. 2016, *ApJ*, 832, 185  
 Lesgourgues, J., & Pastor, S. 2014, *NJPh*, 16, 065002  
 Lopes, R. C. C., Voivodic, R., Abramo, L. R., et al. 2018, *JCAP*, 2018, 010  
 Lopes, R. C. C., Voivodic, R., Abramo, L. R., et al. 2019, *JCAP*, 2019, 026  
 Nojiri, S., Odintsov, S. D., & Faraoni, V. 2018, *PhRvD*, 98, 024005  
 Pavlidou, V., Tetradis, N., & Tomaras, T. N. 2014, *JCAP*, 2014, 017  
 Pavlidou, V., & Tomaras, T. N. 2014, *JCAP*, 2014, 020  
 Peel, A., Pettorino, V., Giocoli, C., et al. 2018, *A&A*, 619, A38  
 Planck Collaboration, Ade, P. A. R., Aghanim, N., et al. 2016, *A&A*, 594, A24  
 Puchwein, E., Baldi, M., & Springel, V. 2013, *MNRAS*, 436, 348  
 Ryu, S., Lee, J., & Baldi, M. 2020, *ApJ*, 904, 93  
 Tyson, J. A. 2002, *Proc. SPIE*, 4836, 10  
 Viel, M., Haehnelt, M. G., & Springel, V. 2010, *JCAP*, 2010, 015  
 Wright, B. S., Koyama, K., Winther, H. A., et al. 2019, *JCAP*, 06, 040